ARTICLE

Lysozyme Catalyzes the Formation of Antimicrobial Silver Nanoparticles

D. Matthew Eby,[†,§,*] Nicole M. Schaeublin,[⊥] Karen E. Farrington,[‡,§] Saber M. Hussain,[⊥] and Glenn R. Johnson[§,*]

[†]Universal Technology Corporation, [‡]Applied Research Associates, Inc., and [§]Microbiology and Applied Biochemistry, Materials and Manufacturing Directorate, Air Force Research Laboratory, 139 Barnes Drive, Suite 2, Tyndall Air Force Base, Florida 32403, and [⊥]Applied Biotechnology Branch, Human Effectiveness Directorate, Air Force Research Laboratory, Wright-Patterson Air Force Base, Ohio 45433

ABSTRACT Hen egg white lysozyme acted as the sole reducing agent and catalyzed the formation of silver nanoparticles in the presence of light. Stable silver colloids formed after mixing lysozyme and silver acetate in methanol and the resulting nanoparticles were concentrated and transferred to aqueous solution without any significant changes in physical properties. Activity and antimicrobial assays demonstrated lysozyme—silver nanoparticles retained the hydrolase function of the enzyme and were effective in inhibiting growth of *Escherichia coli*, *Staphylococcus aureus*, *Bacillus anthracis*, and *Candida albicans*. Remarkably, lysozyme—silver nanoparticles demonstrated a strong antimicrobial effect against silver-resistant *Proteus mirabilis* strains and a recombinant *E. coli* strain containing the multiple antibiotic- and silver-resistant plasmid, pMG101. Results of toxicological studies using human epidermal keratinocytes revealed that lysozyme—silver nanoparticles are nontoxic at concentrations sufficient to inhibit microbial growth. Overall, the ability of lysozyme to assemble silver nanoparticles in a one-step reaction offers a simple and environmentally friendly approach to form stable colloids of nontoxic silver nanoparticles that combine the antimicrobial properties of lysozyme and silver. The results expand the functionality of nanomaterials for biological systems and represent a novel antimicrobial composite for potential aseptics and therapeutic use in the future.

KEYWORDS: antimicrobial · lysozyme · silver · nanoparticle · biocompatibility · biomineralization

Prevalent in a wide range of products, silver has become the most abundant nanoparticulate material used today in the medical and health care fields.[1,2] Added to wound dressings, topical creams, antiseptic sprays, and fabrics, silver functions as an antiseptic and displays a broad biocidal effect against microorganisms through the disruption of membrane function and enzyme activity.[3−5] Whether supplied as a cation, in the elemental state, or part of composite materials, silver ions will destabilize and increase permeability of bacterial membranes, inactivate essential respiratory enzymes and proteins responsible for RNA and DNA replication, and disrupt ion transport processes.[6−8] Though silver will indiscriminately form complexes with several different amino acids and thereby inhibit protein function, it exhibits limited toxicity to mammalian cells.[6] Because of these distinct properties, a myriad of studies have emerged in recent years that focus on the rapid and efficient synthesis of silver nanoparticles for incorporation into medical dressings and devices.[9−11] Among these methods, natural systems that reduce silver ions and form nanoparticles at physiological conditions show promise of generating large amounts of antimicrobial silver colloids inexpensively, and with limited energy input and impact to the environment.[12]

Silver nanoparticle synthesis is mediated by a diverse range of biosynthetic mechanisms, including several examples of fortuitous silver nanoparticle formation by microorganisms, despite a common sensitivity to silver exposure.[13] An early report described a *Pseudomonas stuzeri* strain isolated from silver mine leachate that reduced high concentrations of silver nitrate, resulting in formation of silver crystals in the periplasm of the strain.[14] Since then, additional bacteria, fungi, and plant extracts have been shown to mediate silver nanoparticle formation (a list can be found in Table 1 of ref 13). On the basis of these biosynthetic mechanisms, engineered proteins, biological scaffolds, and phage display techniques have also been explored to direct the molecular control of silver nanoparticle formation.[15−17] These types of applications expand the utility of materials by associating useful biomolecules with inorganic compounds to merge the functional properties of each component into one composite.

Previous work in our laboratory showed that the enzyme lysozyme mediates the synthesis of silica and titania nanoparticles and that the antimicrobial enzyme activity is retained in the inorganic oxide nanoparticles.[18] Lysozyme is present in nature as

*Address correspondence to matt.eby.ctr@tyndall.af.mil, glenn.johnson@tyndall.af.mil.

Received for review January 27, 2009 and accepted March 24, 2009.

Published online April 3, 2009. 10.1021/nn900079e CCC: $40.75

part of the innate immune system in higher organisms and primarily acts against bacteria through enzymatic hydrolysis of the peptidoglycian layer that surrounds the cell membrane. To further explore mechanisms of nanoparticle formation and expand the repertoire of antimicrobial materials, we investigated methods to integrate lysozyme with silver to form multifunctional antimicrobial agents. Using lysozyme as the catalyst, preparations of silver nanoparticles were synthesized and the physical and chemical properties were assessed to characterize the functionality of these hybrid bioinorganic composites. The material was also incubated with a variety of bacterial strains to determine if the antimicrobial properties of lysozyme, as well as the biocidal effects of silver, were retained in these new bionanocomposites. Furthermore, lysozyme−silver nanoparticles were tested in tissue culture viability assays to determine the toxicological effects against mammalian cells.

RESULTS AND DISCUSSION

Synthesis of Lysozyme-Silver (Ag−lyso) Nanoparticles in Methanol. Lysozyme catalyzed silver nanoparticle formation by acting as the sole reducing and nucleating agent. Saturated solutions of protein and silver acetate in methanol were mixed at varying molar ratios and silver nanoparticles formed when exposed to light (Figure 1). Particles formed in less than an hour and, to a limited extent, their size distribution and monodispersity can be controlled by the Ag^+/lysozyme molar ratio. At lower Ag^+/lysozyme molar ratios (*e.g.*, preparation I), particles were smaller and more monodispersed than nanoparticles formed at the higher Ag^+/lysozyme molar ratio (*e.g.*, preparation II). The yellow color and the symmetrical plasmon resonance absorption band centered at 420 nm in the UV−vis spectrum of preparation I is indicative of small and uniform nanoparticle size distribution.[19] In preparation II, the increased number of silver particles and their variation in size caused a broadening of the plasmon band and a corresponding color change from yellow to red in the visible spectrum. Nanoparticles did not form in the absence of light (not shown) and when silver or lysozyme was omitted from the solution, as no color or UV−vis absorbance change was observed in these wells of the microtiter plate (far left and far right wells in Figure 1A). Also, a colloidal suspension of nanoparticles did not form under aqueous conditions. When the reaction was completed in water, a brown to gray-colored precipitate formed in the bottom of microtiter plate wells. Nanoparticles were observed in the precipitate, but they ranged broadly in size and shape. In addition, the preparation did not exhibit a distinctive surface plasmon resonance absorption band in the visible range (Figure S1 in Supporting Information).

Dynamic light scattering (DLS) was employed to obtain quantitative size distributions and a more precise

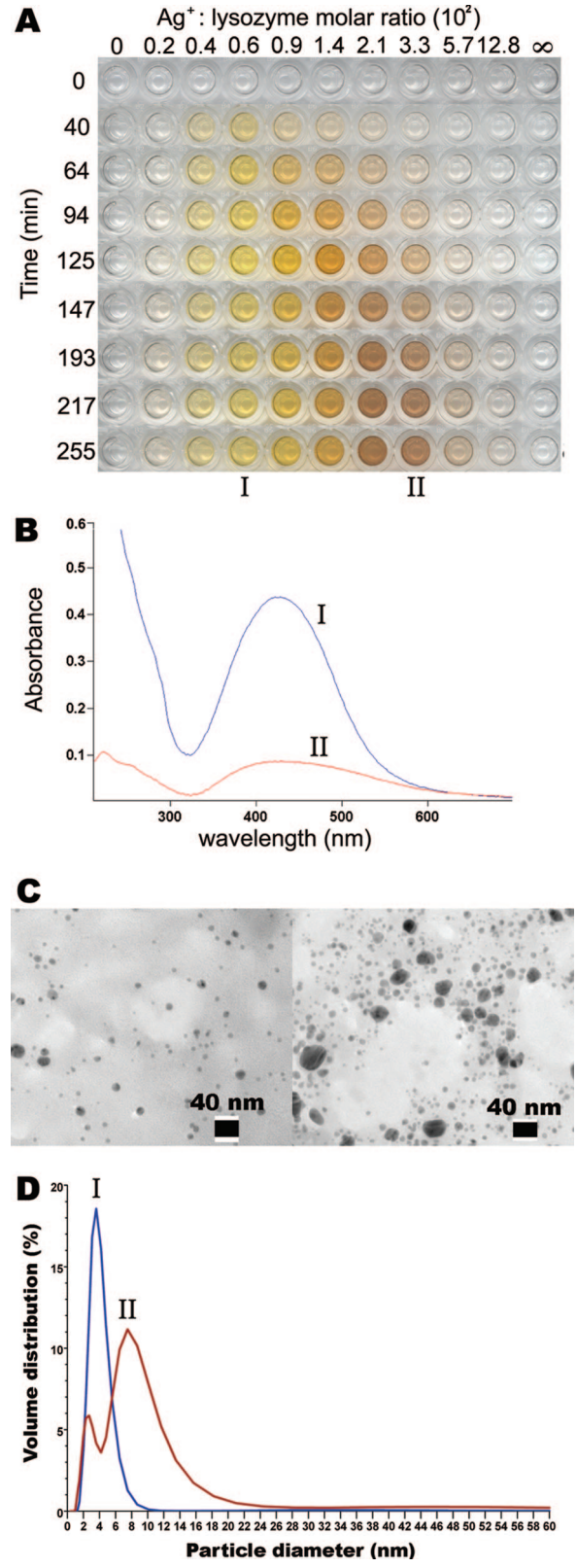

Figure 1. Lysozyme and silver acetate solutions were mixed in varying molar ratios and exposed to light over the course of 255 min. At set time intervals, reactions were added to a row of microtiter plate wells and imaged using a document scanner (A). Representative samples of yellow (I) and red (II) nanoparticles from the synthesis assay were used in absorbance spectroscopy (B), TEM imaging (C), and dynamic light scattering to determine nanoparticle size distribution (D).

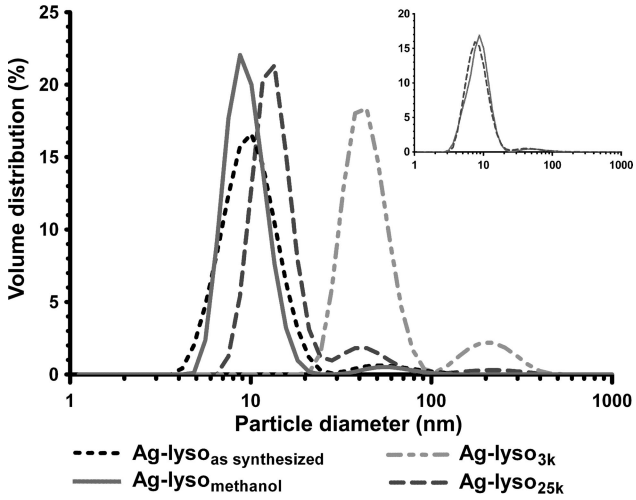

Figure 2. Nanoparticle size distribution of methanolic and aqueous Ag−lyso preparations using DLS. Nanoparticles were prepared as described in the Materials and Methods. Inset: Size distribution of 6 month preparations of Ag−lyso$_{methanol}$ and Ag−lyso$_{25k}$

measure of monodispersity in silver nanoparticle solutions. A comparison between the size distribution histograms of preparations I and II show a decreased fraction of particles in the smaller peak mean size in preparation II, concurrent with the presence of a major peak mean at a larger nanoparticle size (between 8 and 12 nm). This result can be explained best by the Ostwald ripening process, where the atoms of smaller, energetically unstable particles will dissipate and coalesce into larger, more stable particles.[20] At low Ag^+/lysozyme molar ratios, silver ions are apparently limiting and the nanoparticle synthesis forms a monodispersed colloidal suspension of smaller nanoparticles. Also at low molar ratio, lysozyme appeared to limit further ripening of smaller particles into larger particles. As the Ag^+ concentration increased respective to lysozyme, the higher Ag^+ concentration allowed for increased particle size and abundance, which led to the agglomeration and the formation of more nonsymmetrical masses before complete nanoparticle maturation. Overall, monodispersity and size control of Ag−lyso nanoparticle suspensions can be achieved by limiting the Ag^+/lysozyme molar ratio. For the remainder of the study, nanoparticle solutions were made from a solution consisting of 25 μg mL^{-1} lysozyme and 42 μg mL^{-1} silver acetate in methanol, which maximized the nanoparticle concentration without significantly reducing the monodispersity of the suspension (similar in composition to the middle well in Figure 1A).

Ag−lyso Nanoparticle Colloidal Stability and Transfer into Aqueous Solutions. In addition to silver reduction and nanoparticle formation, lysozyme acted as a capping agent to stabilize the colloidal suspensions and limit agglomeration. Lysozyme is a highly cationic and amphiphilic protein that will adsorb to ionic and hydrophobic surfaces, including metal surfaces.[21−24] After synthesis in methanol, lysozyme-stabilized nanoparticle suspensions could be concentrated approximately 100-fold (up to 1 mg mL^{-1}) with no noticeable precipitation. Furthermore, when concentrated solutions were transferred into water by dialysis, no visible precipitation of nanoparticles was noted during the process. This result is significant, as the strong ionic interactions between metal nanoparticles normally make it difficult to achieve high concentrations of monodispersed and stable colloids in water.[25,26] To further assess the importance of lysozyme as a surfactant in aqueous solutions, different molecular weight cutoff (MWCO) membranes were used during dialysis to either retain (3000 MWCO) or remove excess and easily diffusible lysozyme (25 000 MWCO) from solutions (preparations designated Ag−lyso$_{3k}$ and Ag−lyso$_{25k}$, respectively). In addition, dialysis was also completed in water containing an ionic detergent (sodium dodecyl sulfate, SDS), in efforts to remove all the lysozyme before transfer into ultrapure water (preparation designated Ag−lyso$_{SDS}$). After the dialysis treatments, lysozyme was detected in each nanoparticle solution (Figure S2 in Supporting Information). ATR FTIR spectrum of the Ag−lyso$_{25k}$ preparations confirmed that lysozyme remained adsorbed to silver nanoparticles when protein was allowed to diffuse through the dialysis tubing, as shown by the characteristic amide I and II vibrations that arose from the peptide backbone. Even after SDS treatment, lysozyme was still detected by ATR FTIR, although the spectrum corresponding to the protein was very weak and illustrates that only trace amounts of lysozyme remained in Ag−lyso$_{SDS}$ preparations. In each aqueous preparation, the dialysis treatment did not noticeably change the size of individual nanoparticles (Figure S3 in Supporting Information). Visual inspection of nanoparticles in TEM images show that the nanoparticles in each aqueous preparation are similar in shape and size.

In addition to TEM imaging, the size distribution and polydispersity of the different preparations were analyzed using DLS (Figure 2). After synthesis, the majority of the nascent nanoparticles measured 10 nm in diameter, while a smaller fraction had a larger mean diameter of 62 nm (Ag−lyso$_{as\ synthesized}$). The size and volume distribution remained the same when the preparations were concentrated in methanol and then diluted with methanol to restore the original concentration (Ag−lyso$_{methanol}$). When Ag−lyso nanoparticles were concentrated and dialyzed into water, the extent of agglomeration was dependent upon the amount of lysozyme present in the preparation. In preparations where lysozyme was retained during dialysis (Ag−lyso$_{3k}$), the concentrated nanoparticles appeared to cluster, forming agglomerates with mean diameters of 45 and 217 nm (Figure 2). When free lysozyme was removed during dialysis so that the only lysozyme present is adsorbed to nanoparticle surfaces (Ag−lyso$_{25k}$), particle size distribution was similar to nascent particles and those in the concentrated metha-

TABLE 1. Surface Charge of Silver Nanoparticle Preparations in Solution

preparation[a]	Ag−lyso methanol	Ag−lyso 25k	Ag−lyso 3k	Ag−lyso SDS
surface charge[b]	+31	+38	+36	−7
s.d.	±2	±2	±1	±1

[a]After synthesis, Ag−lyso nanoparticles were either concentrated 100-fold in methanol (Ag−lyso methanol) or prepared as stated in Materials and Methods. [b]Measured as the zeta potential (mV); s.d. = standard deviation.

nol suspensions. When preparations were treated to disassociate the lysoyzme from the nanoparticles (Ag−lyso$_{SDS}$), the nanoparticles agglomerated rapidly and formed large clusters that could not be accurately measured by DLS (data not shown). As a result, Ag−lyso$_{SDS}$ preparations were highly unstable and would not maintain a colloidal suspension. Conversely, the other aqueous and methanolic preparations would remain stable in a concentrated form for months with minimal precipitation, although Ag−lyso$_{3k}$ preparations would turn cloudy after several weeks. This observation was consistent with a previous study of lysozyme-stabilized gold nanoparticles, where it was assumed that excess lysozyme in nanoparticle preparations slowly denatures during storage to yield the cloudy appearance.[27] Overall, the concentrated methanolic and Ag−lyso$_{25k}$ preparations were the most stable preparations. Even after 6 months of storage at room temperature, the two preparations retained a consistent mean size and monodispersity that was comparable to the nascent nanoparticles (Figure 2 inset). Hence, these treatments were considered optimal for generating concentrated stocks of silver nanoparticles in methanol and in water.

Surface Potential of Ag−lyso Nanoparticles. The difference in potential between the colloidal suspension medium and the surface charge of the particle (measured as the zeta potential in mV) not only provides a quantitative value for the overall surface charge of the nanoparticles, but is also an indicator to predict colloidal stability.[28] A higher absolute zeta potential suggests a greater electrostatic repulsion between particles and, therefore, a lower incidence of agglomeration and more stable colloidal suspension. A value of approximately |30| mV has been established as a theoretical limit to colloidal stability. For example, zeta potential values of −29 and 40 mV have been measured for colloidal silver nanoparticles suspensions that contain the commonly used surfactants citrate and cetyltrimethylammonium, respectively.[28,29] As shown in Table 1, zeta potential measurements of the methanolic and three aqueous Ag−lyso preparations are consistent with their colloidal stability. The stable Ag−lyso suspensions in methanol and water exhibited zeta potentials above the threshold for colloidal stability. The Ag−lyso$_{SDS}$ nanoparticles exhibited a weak negative surface charge, due to the adsorption of anionic SDS molecules on nanoparticle surface. Consistent with its observed colloidal instability, the measured surface potential of Ag−lyso$_{SDS}$ nanoparticles was well below |30| mV.

Estimation of the Lysozyme Coating Thickness on Ag−lyso$_{25k}$ Nanoparticles. The thickness of the lysozyme coating on silver nanoparticles was estimated by comparing the average nanoparticle diameters independently determined from DLS and TEM image analysis. Due to the relationship between particle size and its speed of Brownian motion (*i.e.*, Stokes−Einstein law), DLS can accurately measure the complete dimension of a nanoparticle in well-dispersed colloidal solutions through fluctuations in light scattering intensity. Alternatively, TEM will only image silver and will render the lysozyme component of nanoparticle nearly transparent. As a result, the difference between these two diameter calculations should equal the thickness of a protein coat on the nanoparticle surface. After measuring over two hundred particles in four separate TEM images of Ag−lyso$_{25k}$ preparations, the mean diameter was determined to be 8 ± 3 nm (size distribution histogram can be found in Supporting Information, Figure S4). As shown in Figure 2, the size distribution mean of the majority of the nanoparticles was 14 ± 4 nm. Curiously, the difference in mean diameters calculated by DLS and from TEM images matches the thickness of a protein monolayer on the silver nanoparticle surfaces. The dimensions of lysozyme are 3.0 × 3.0 × 4.5 nm and a protein monolayer on the nanoparticle would be two times the diameter of lysozyme or approximately 6 nm.[30] Accordingly, the estimated layer thickness based on DLS and TEM differences should be viewed with some scrutiny, owing to considerable differences in measuring methods and the very small disparity between the diameters. However, the result is consistent with another study that also concluded lysozyme forms an adsorbed monolayer on the surface of gold nanoparticles.[27] In addition, all but one nanoparticle were found in TEM images to be <20 nm in diameter, suggesting the large mean peak area observed in DLS size distributions of Ag−lyso$_{25k}$ preparations are clusters of nanoparticles and not single nanoparticles of a larger diameter. Taken together, the results suggest lysozyme forms a tightly associated monolayer on nanoparticle surfaces, which is responsible for inhibiting further Ostwald ripening and providing a lasting monodispersity to colloidal solutions.

Effect of Silver Nanoparticle Synthesis on Lysozyme. The native hydrolytic activity of lysozyme was not inhibited after mixing with silver ions in methanol and after nanoparticle formation (Table 2). Enzyme activity was confirmed by the hydrolysis of the synthetic membrane mimic, *p*-nitrophenyl penta-*N*-acetyl-β-chitopentaoside. Hydrolase activity did not decrease after mixing with silver ions and methanol and after nanoparticle formation. According to previous reports, lysozyme is partially denatured in organic solvents and

TABLE 2. Effect of Silver on Hydrolytic Activity of Lysozyme

solution components[a]	lysozyme	Ag^+ and lyso dark	Ag−lyso light	Ag^+
relative activity[b]	0.115	0.146	0.119	0.001
s.d.	±0.006	±0.005	±0.01	±0.001

[a]Preparations consisted of the following: 5 mg mL^{-1} lysozyme (lysozyme); 5 mg mL^{-1} lysozyme and 0.5 mM silver acetate in 50% methanol incubated at room temperature for 16 h in the absence and presence of light (Ag^+ and lyso dark and Ag−lyso light, respectively); 0.5 mM silver acetate in 50% methanol (Ag^+); s.d. = standard deviation. See Materials and Methods for more details. [b]Activity of lysozyme was determined colorimetrically by hydrolysis of the synthetic membrane mimic *p*-nitrophenyl β-glycoside of *N*-acetylchitooligosaccharide as previously reported.[48] Stock solutions were diluted 1000-fold into assay buffer before analysis. Activity rates were measured in $\Delta Abs_{405nm}\ h^{-1}$.

dissolution in methanol will alter the tertiary structure of the protein.[31] In addition, silver ions are known to bind nonspecifically to proteins by interacting with many different amino acid side groups.[6,32] In many cases, these interactions will inhibit enzyme activity and denature the protein. While the assay conditions could not confirm that lysozyme was active in the presence of high silver concentrations and methanolic solutions (preparations were diluted 1000-fold into activity assay buffer), the results show that exposure to silver ions, initial dissolution into methanolic solutions, and subsequent synthesis of silver nanoparticles do not irreversibly denature the protein.

Antimicrobial Activity of Ag−lyso Nanoparticles. The silver nanoparticles exhibited antimicrobial activity against three representative bacterial strains and one fungal strain (Table 3). In all assays, Ag−lyso preparations were comparable, if not superior biostatic agents to silver acetate. Under our conditions, lysozyme alone had no effect on any of these strains when it was used as the sole antimicrobial agent. Silver acetate exhibited potency

TABLE 3. Minimum Inhibitory Concentrations (MIC) of Ag−lyso Preparations

preparation[a]	Ag−lyso 3k	Ag−lyso 25k	Ag−lyso SDS	Ag^+	lysozyme
E. coli, ATCC 25922	3.5[b]	1.7	2.5	5.6	>1000
s.d.	±1.1	±0.7	±0	±2.1	±0
S. aureus, ATCC 25923	3.9	1.9	2.9	20	>1000
s.d.	±0.9	±0.6	±1.7	±11	±0
B. anthracis, Sterne strain 34F2	7.7	3.0	7.5	39	>1000
s.d.	±1.7	±1.1	±6.7	±25	±0
C. albicans, ATCC 10231	25	19	4.1	89	>1000
s.d.	±22	±24	±1.2	±35	±0

[a]Ag−lyso preparations are as described in Materials and Methods. Freshly prepared stock solutions of 3.6 mg mL^{-1} silver acetate in water (Ag^+) and 10 mg mL^{-1} lysozyme in water (lysozyme) were also used in assays; s.d. = standard deviation. [b]Concentrations are μg mL^{-1}.

that approached that of the Ag−lyso nanoparticles, which suggested that silver plays a determinant role in the antimicrobial mechanism of the nanoparticles. The dialysis procedures intended to remove unassociated lysozyme did not substantially alter the effectiveness of the Ag−lyso preparations toward the bacterial strains. Each Ag−lyso suspension was comparable as an antibiotic, even though the amount of lysozyme, surface charge, and their degree of agglomeration varied between the preparations. Overall, there was no clear correlation between the measured potency of the silver nanoparticles and the effective size of the particles in solution or their surface charge. Comparable activity was unexpected, because previous work by others showed that particle size and rate of agglomeration affected potency.[5,33,34] One possible explanation is that the size and agglomeration measurements completed on the Ag−lyso preparations do not reflect the dispersity of the nanoparticles in the assay. Once diluted into assay buffer, physical characteristics of the nanoparticles are influenced by cellular interactions and the culture media. Alternatively, the dialysis treatment revealed a subtle difference in assays using *C. albicans* as the test strain, where removal of lysozyme from the nanoparticles improved the biostatic properties. The differences in MIC values between the Ag−lyso preparations in *C. albicans* assays may be influenced by a combination of factors, including structural composition, adsorption properties, electrostatic forces and/or enzymatic properties of yeast cell surfaces. One, or a combination of the differences, may have reduced the effectiveness of coated silver nanoparticles against *C. albicans* compared to the bacterial strains.

The effect of Ag−lyso nanoparticles on the *B. anthracis* Sterne strains was visualized using AFM (Figure 3). After a 2.5 h incubation in the presence of nanoparticles, weakened and partially destroyed cell envelopes were apparent when compared to the intact chains of cells evident in control samples. Cells exposed to nanoparticles were also noticeably aggregated in the images, where chains of cells had laterally adsorbed to each other. This type and degree of aggregation was abundant with treated cells and rarely seen in AFM and light microscope images of normal cells. Upon closer inspection of the image, treated cell surfaces appear to be covered in spherical protrusions that correspond to the sizes of Ag−lyso nanoparticles. Adsorption of silver nanoparticles to cell membranes was expected and most likely promoted the lateral adsorption of multiple cell chains. Cell surfaces of untreated and treated cells were scanned at a higher resolution and amplitude error images were obtained to show relative roughness. Treated cell surfaces were mottled with spherical aggregates that corresponded to the approximate size of Ag−lyso nanoparticles. In contrast, the surfaces of untreated cells were relatively smooth and appeared structurally intact. Overall, the images are consistent

with nanoparticle adsorption and destruction to cellular membranes in the presence of Ag−lyso$_{25k}$ preparations.

Surprisingly, Ag−lyso$_{25k}$ nanoparticles demonstrated a significantly lower minimum inhibitory concentration over silver acetate against silver-resistant strains of *P. mirabilis* (LST149 and LST169A) and a recombinant *E. coli* strain (J53) containing the antibiotic- and heavy metal-resistant plasmid pMG101 (Table 4). These strains are normally highly resistant to Ag^+, yet, when exposed to Ag−lyso$_{25k}$ preparations, the composite nanoparticles inhibited growth at concentrations comparable to the silver-sensitive strains listed in Tables 3 and 4. In addition, J53(pMG101) was shown to be sensitive to lysozyme alone (MIC = 63 μg mL^{-1}), compared to strain J53 without the silver-resistance plasmid. This is an interesting result, as it demonstrated sensitivity to lysozyme when the plasmid is present in the strain. While these preliminary results do not unequivocally show that silver resistance confers lysozyme sensitivity, it does raise questions to whether the antibiotic resistance mechanisms encoded on pMG101 significantly alter cellular properties to the extent that pathogens harboring this plasmid would be vulnerable to other antibiotic treatments. Further discussion on this topic is included in the Conclusions section.

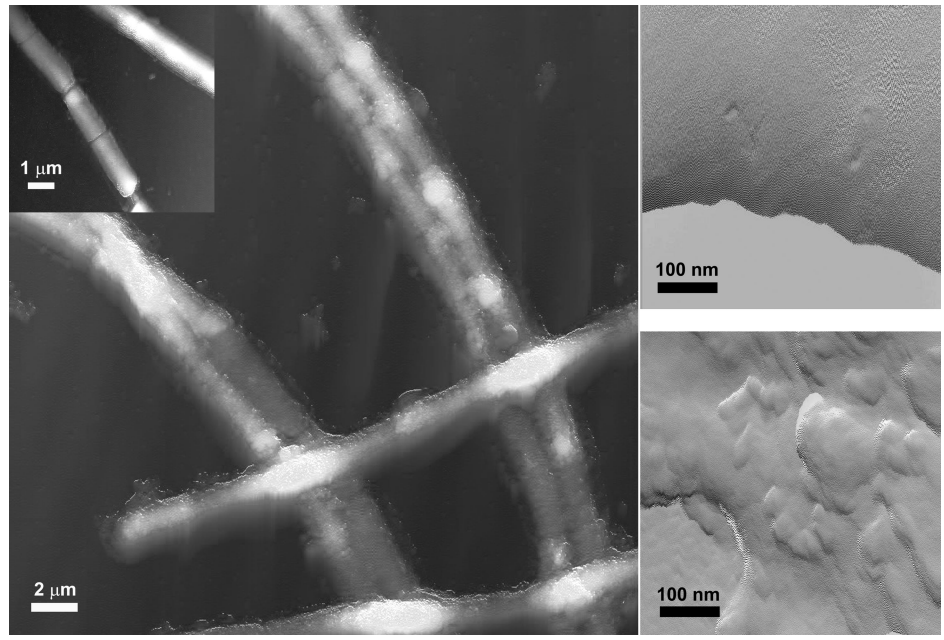

Figure 3. AFM composite images of *B. anthracis* strain Sterne before and after exposure to Ag−lyso nanoparticles. Untreated *B. anthracis* cells are shown in inset (top left) and cells after 2.5 h incubation with Ag−lyso nanoparticles are shown in the larger image on left. Height from base (black) to top of cell (white) is approximately 500 nm. AFM amplitude error images showing cell surfaces of untreated cells (top, cell surface is shown in upper region of image) and after exposure to Ag−lyso nanoparticles (bottom) are shown on the right.

Toxicology of Ag−lyso$_{25k}$ Nanoparticles. Results from *in vitro* tissue culture assays revealed that the nanoparticle composite material caused no measurable toxicological effect against mammalian cells at concentrations necessary to inhibit bacterial growth. A human epidermal keratinocyte cell line (HaCaT) was chosen based on its relevance to numerous consumer products that incorporate silver as antimicrobial agents and come into close contact with the skin (*e.g.*, wound dressings, skin sanitizers, and textiles).[1] Ag−lyso$_{25k}$ nanoparticles were incubated with the cells and mitochondrial function was measured to determine viability following exposure (Figure 4). The results demonstrated there was no significant difference in the viability between control cells and cells treated with up to 25 μg mL^{-1} nanoparticles. At higher silver concentrations, cell viability dropped to 30% of the untreated control. The MIC required to kill most of the microbial strains used in this study were below concentrations that are toxic to HaCaT cells (Tables 3 and 4).

The results support the potential therapeutic application of the Ag−lyso nanoparticles over conventional nanoparticle preparations. Previous studies reported that commercially prepared silver nanoparticles caused significant effects in mitochondrial function at concentrations below 25 μg mL^{-1}.[35−37] The comparative decrease in toxicity of Ag−lyso$_{25k}$ nanoparticles was simi-

TABLE 4. Minimum Inhibitory Concentrations of Ag−lyso Nanoparticles against Silver-Resistant Bacterial Strains

Preparation[a]	Ag−lyso 25k	Ag^+	lysozyme
J53[b]	0.8[c]	11	>1000
s.d.	±0.6	±5.1	±0
J53(pMG101)	2.6	>1000	63
s.d.	±1.0	±0	±0
P. mirabilis, ATCC 29906	1.7	1.8	>1000
s.d.	±1.0	±0.8	±0
LST149[d]	8.4	>1000	>1000
s.d.	±2.2	±0	±0
LST169A[d]	2.2	>1000	>1000
s.d.	±1.4	±0	±0

[a] Ag−lyso$_{25k}$ was prepared as described in Materials and Methods. Freshly prepared stock solutions of 3.6 mg mL^{-1} silver acetate in water (Ag^+) and 10 mg mL^{-1} lysozyme in water (lysozyme) were also used in assays; s.d. = standard deviation. [b] *E. coli* strain J53, with and without silver resistance plasmid, pMG101. See text for source and description. [c] Concentrations are μg mL^{-1}. [d] *P. mirabilis* heavy metal resistance strains. See text for source and description.

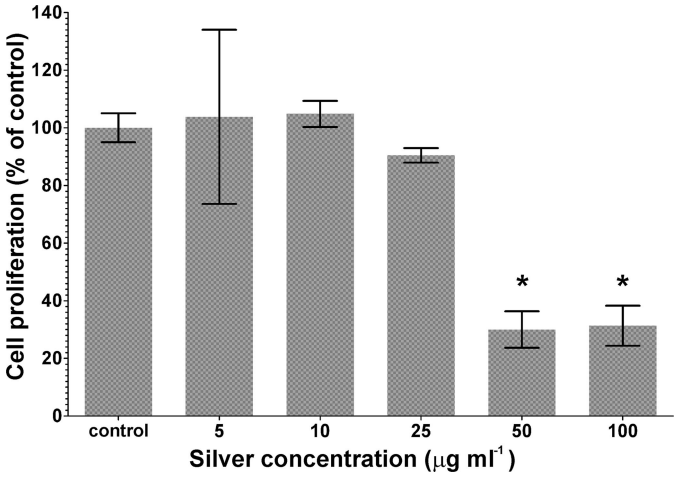

Figure 4. Viability of HaCaT cells treated with Ag−lyso$_{25k}$ nanoparticles. Cell proliferation was determined by measuring metabolic activity of cell cultures after 24 h incubation with nanoparticles and compared against non-nanoparticle control cultures. The asterisk (*) denotes significance compared to control values ($p < 0.05$).

lar to that also measured for polysaccharide-coated silver nanoparticles over commercially prepared silver nanoparticles.[37] In another study, starch-coated silver nanoparticles also did not affect viability of human lung fibroblast cells at or below 25 μg mL^{-1} in a 24 h time period.[38] An increase in reactive oxygen species was observed at 25 μg mL^{-1}, well as some evidence of DNA damage, although lower concentrations of silver nanoparticles were not tested for these particular assays. Overall, the initial results reported here are promising, but additional toxicological assays are needed to understand the full effect of the composite to human health.

CONCLUSIONS

A comprehensive series of morphological and electrostatic measurements on the Ag−lyso preparations revealed a set of physical and chemical properties, which provided insight to the formation of the biocomposite material (Figure 5). On the basis of the observations, we propose that lysozyme takes on a unique amphipathic form in methanol that permits silver reduction and directs nanoparticle formation to yield stable silver colloids. In methanol, protein conformation will undoubtedly be different than proteins in aqueous solvents. Though the specific mechanism by which lysozyme is able to reduce silver remains a mystery, one hypothesis is that the altered structure contributes to the synthesis of stable and monodispersed colloids. Silver reduction occurs when the reaction is completed with lysozyme in water (as shown by the aggregated, brown-gray product), but the product readily precipitated from solution and never formed a colloidal suspension. This is consistent with previous reports that show stable and monodispersed suspensions of metal nanoparticles are difficult to achieve with aqueous-based synthesis, because water facilitates strong ionic interactions between forming particles.[25] The hydrophobicity of methanol is a major factor in stabilizing silver colloids by reducing nanoparticle adsorption and agglomeration, but why then is colloidal stability retained to such a high degree after dialysis into water? The unique complex that forms between lysozyme and silver in methanol must be crucial to colloidal stability of the suspension after transfer into water. It is known that dissolution of lysozyme in solutions of ≥50% methanol causes partial denaturation of the protein, leading to a unique globular state.[31] It is plausible that the rearrangement in tertiary structure exposes additional hydrophobic residues to the solvent that are normally packed within the protein core under aqueous conditions. Lysozyme is also a highly cationic protein and, in a globular state, the protein would take on a new cationic and amphiphilic form. In this uniquely amphipathic state, the lysozyme coating on the particle may impose a positive-positive charged-induced and/or a hydrophobic-induced repulsion between nanoparticles. Hence, the altered protein conformation may enhance the surfactant properties of lysozyme in methanol. After solvent exchange with water, interactions between the protein and the nanoparticle may be stabilizing the unique form of lysozyme and the protein continues to act as a surfactant in aqueous conditions.

In most cases, perturbation of native protein structure will lead to inactivation of enzyme activity. Dissolution into organic solvents and exposure to ionized heavy metals are certain ways to denature, precipitate, and inactivate most proteins. Here, lysozyme is an exception, where the protein retains hydrolytic activity after exposure to methanol and silver ions and after nanoparticle synthesis. The anomaly can be explained by at least two possibilities. First, the altered structure that allows lysozyme to function as a surfactant may not affect enzymatic activity. In its native conformation, lysozyme is highly amphiphilic and contains a patchwork distribution of cationic and hydrophobic residues over the solvent accessible surface.[39] These characteristics may largely contribute to the surfactant properties of lysozyme and the altered structure imposed by methanol may be minimal and not affect the catalytic active site. Conversely, studies on methanol-induced lysozyme transitions have demonstrated distinctly different secondary and tertiary conformation in methanolic solutions, which likely inactivates activity.[31,40] A second possibility is more plausible and is based on refolding characteristics of lysozyme. Used in numerous kinetic folding assays, lysozyme has been shown to denature and refold under a variety of conditions with 100% retention of activity.[41] Solvent-induced transitions will disrupt secondary and tertiary structure, but the protein rapidly refolds back to it native state after dissolution in aqueous media. If the methanolic form of lysozyme is inactive, dilution into the aqueous buffer may cause lysozyme to partially or completely revert to

its native conformation and act as a hydrolase (as demonstrated in our enzymatic activity assays), yet still remain adsorbed to nanoparticle surfaces and retain effective surfactant properties. Unfortunately, the hydrolytic assay requires aqueous buffer and the activity of the methanolic form of lysozyme cannot be tested under the experimental conditions. Determination of lysozyme structure in Ag−lyso preparations by NMR would be advantageous to better elucidate the unique structure−function relationships of the enzyme in methanol.

The amount of lysozyme in the aqueous preparations further influences colloidal stability. When excess lysozyme was retained after dialysis (Ag−lyso$_{3k}$), soluble protein may have reverted back to its native conformation and caused nanoparticles to agglomerate, but not to a degree that overcame colloidal stability. In the native form, the free protein acted as a "glue" to form large clusters of nanoparticles, as shown by the increased size distributions using DLS. Once this glue was removed from solution after dialysis (Ag−lyso$_{25k}$), the lysozyme remaining on nanoparticle surfaces retained surfactant properties and the preparations were concentrated, stored, and reused at a wide range of concentrations in water without altering the physical properties of nanoparticles. Under our conditions, lysozyme is required for colloidal stability and acted as a better stabilizer than SDS. Once the majority of lysozyme was removed from the preparation and replaced with SDS, preparations became unstable and nanoparticles agglomerated and precipitated.

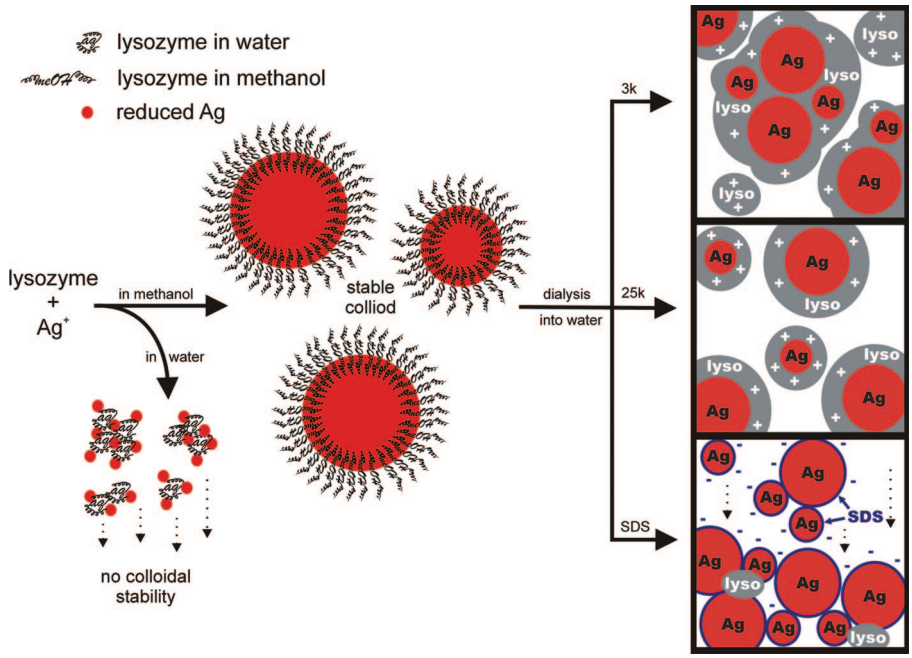

Figure 5. Proposed mechanism of Ag−lyso nanoparticle formation.

Ag−lyso nanoparticles inhibited growth of the selected microorganisms and were highly effective against silver-resistant bacterial strains. The findings are particularly relevant to the rise of antibiotic-resistant pathogens in health care, because the silver-resistant strains chosen in our study are representative of bacteria that cause persistent infections in hospitals and have also acquired antibiotic resistance through natural selection. *E. coli* and *P. mirabilis* are frequent etiologic agents in catheter-associated urinary tract infections, which are the most common type of nosocomial infections in hospitals and nursing homes.[42] The heavy metal-resistant strains LST149 and LST169A are members of the Primate Amalgam Collection, which is a collection of fecal bacteria isolates that acquired heavy metal and multiple antibiotic resistance through the selective enrichment of mobile genetic elements in the oral and intestinal microflora of primates with mercury- and silver-containing dental amalgam fillings.[43,44] The plasmid pMG101, originally isolated from a *Salmonella typhimurium* strain that killed several patients in a hospital burn ward, confers heavy metal resistance as well as multiple antibiotic resistance to a variety of bacterial strains.[45] These strains represent an emerging threat where mobile genetic elements that confer antibiotic resistance are proliferating in the microflora of humans and in health care environment through natural selection.[1,46] Currently, the biocidal mechanism of Ag−lyso nanoparticles against the LST strains is unknown, but a hypothesis can be derived from the unique sensitivity observed with J53(pMG101), because the genotype and method of antibiotic resistance is known for this strain. The plasmid encodes for a system of membrane-bound proteins that function collectively as heavy metal efflux pumps.[47] Production of these proteins may alter the cellular membrane so that it is more susceptible to lysozyme activity. Thus, the combined action of lysozyme and silver may overcome silver-resistance mechanisms to effectively inhibit growth of the strain. If this is true, then Ag−lyso preparations will limit further dissemination of silver resistance among pathogenic microorganisms in the environment by blocking the selective enrichment of resistant organisms. Overall, the results presented here are preliminary and additional studies are necessary to further understand the mechanism of silver and lysozyme susceptibility among antibiotic resistant strains.

The use of lysozyme in silver nanoparticle formation offers several advantages over many inorganic syn-

thesis reactions. The process offers a simple, inexpensive, and passive method to generate large amounts of stable silver colloids. Biological routes of nanoparticle synthesis are of increasing interest as they tend to be less energy-intensive and more environmentally friendly than conventional synthetic methods. Hen egg white lysozyme is widely used in food processing and preservation, and its use as the reducing agent and surfactant for silver nanoparticle preparation is a new advance for the development and subsequent transition of Ag−lyso preparations to applications in these types of industries where either lysozyme or silver is already prevalent. By and large, the rise of multiple antibiotic resistant bacterial strains drives a continuous search for novel antimicrobial agents and new methods to inhibit bacterial growth. The ultimate goal is to develop a potent, safe, cost-effective, easily synthesized and readily available alternative to conventional antibiotics that are becoming ineffective against multiresistant pathogens at an alarming pace. The bioinorganic composites presented here represent an alternative material that addresses issues in the application of silver nanoparticles for aseptic and therapeutic use and will hopefully help reduce the propagation of antibiotic-resistance pathogens in the future.

MATERIALS AND METHODS

Reagents and Chemicals. Hen egg white lysozyme (~95%, ~50 000 units/mg protein) and silver (I) acetate (99.99%) were obtained from Sigma-Aldrich (St. Louis, MO). *p*-Nitrophenyl-penta-*N*-acetyl-β-chitopentaoside (PNP-$(GlcNAc)_5$) was synthesized by Seikagaku Corp., (Tokyo, Japan). Silver nanoparticles averaging 55nm diameter were purchased from Nanotechnologies Inc. (Austin, TX.) All other chemicals and reagents not specifically listed were obtained from either Sigma-Aldrich or through Fisher Scientific (Pittsburgh, PA) and were of the highest purity available.

Synthesis of Ag−lyso Nanoparticles. Lysozyme and silver acetate were added in excess of their solubility to separate volumes of 100% methanol and stirred for 16 h in the absence of light. After mixing, the solutions were centrifuged for 5 min at 5000*g* to remove any remaining insoluble material and the supernatants were mixed together in a series (10:0, 9:1, 8:2,..., 1:9 and 0:10; v:v) and incubated at room temperature for approximately 4 h on top of a fluorescent light box (X-ray Film Illuminator, model 1417-1, Spectronics Corp., Westbury, NY). During incubation, 100 μL aliquots of the reaction mixtures were placed in a microtiter plate and imaged using a document scanner. After nanoparticles developed, the silver−lysozyme nanoparticle suspensions were either used immediately or stored at room temperature in the dark until use. A similar procedure was also completed in water using a range of lysozyme and silver acetate concentrations as described for the methanolic solutions.

For additional physical and chemical analysis, antimicrobial assays, and toxicological evaluation, a solution of 84 μg mL^{-1} silver acetate in methanol was added to a 50 μg mL^{-1} lysozyme solution in methanol (1:1, v:v) and incubated in the presence of light for 24 h to induce silver nanoparticle formation (designated as Ag−$lyso_{as\ synthesized}$). Lysozyme was first dissolved in a few drops of water before mixing with methanol to aid in dissolution (volume of water was <1% in final preparation). After formation, the nanoparticle preparations were concentrated approximately 100-fold in an Amicon stirred cell filtration device (Millipore Corp., Bedford, MA) using a 30 000 molecular weight cutoff (MWCO) filter (designated as Ag−$lyso_{methanol}$). The silver−lysozyme nanoparticle mixtures were then dialyzed in the dark against two changes of 4 L deionized water for 24 h in either 3000 MWCO or 25 000 MWCO dialysis tubing (Spectra/Por cellulose ester, Spectrum Medical Industries, Houston, TX) and designated as preparations Ag−$lyso_{3k}$ and Ag−$lyso_{25k}$, respectively. Dialysis was completed in order to remove the methanol and impurities from the Ag−lyso suspensions. Dialysis in 25 000 MWCO tubing was also completed to remove protein that was not associated with the silver nanoparticles. An additional preparation was synthesized as above and treated with the intention to strip away any lysozyme that is not tightly associated to the nanoparticles. Following synthesis, preparations were transferred to 25 000 MWCO dialysis tubing and then dialyzed against two changes of 5% sodium dodecyl sulfate (SDS, 4 L) for 48 h and then in two changes of water (4 L) for 48 h (preparations designated as Ag−$lyso_{SDS}$). Final aqueous preparations were maintained at room temperature and in the dark until use. The concentration of silver in saturated methanol solutions and in each nanoparticle preparation was determined using inductively coupled plasma-optical emission spectrometry at the Chemical Analysis Laboratory, University of Georgia (Athens, GA). Concentration of saturated lysozyme in methanol was determined using a spectrophotometer to measure absorbance at 280 nm and comparison to absorbance of known standards in methanol.

Ag−lyso Nanoparticle Characterization. Spectroscopic analysis was accomplished using a Cary 3E spectrophotometer (Varian Inc., Palo Alto, CA) with 0.5 mL quartz cuvettes. TEM was completed using a 100 CX II electron microscope from JEOL Ltd. (Tokyo, Japan). Nanoparticle diameters calculated from TEM images were completed using ImageJ processing and analysis software (version 1.38, National Institutes of Health, USA). Nanoparticle size and surface charge measurements were determined using a Zetasizer nano CZ90 (Malvern Instruments Ltd., Worchestershire, UK). Size was measured by dynamic light scattering (detector angle: 90°) using a 633 nm wavelength laser and the following refractive index (η_i) and viscosity (μ, in cP) values: particle $\eta_i = 0.54$; methanol, $\eta_i = 1.326$, $\mu = 0.5476$; water, $\eta_i = 1.330$, $\mu = 0.8872$. Surface charge was measured by electrophoretic mobility coupled with laser Doppler velocimetry and calculated as the zeta potential using the Smoluchowski equation:

$$\text{zeta} = U\eta / \varepsilon$$

where zeta is the zeta potential, U is the electrophoretic mobility, η is the medium viscosity, and ε is the dielectric constant. Analysis was completed at 25 °C and each reported measurement is an average of at least six independent samples and between 12 and 20 measurements of each sample. Attenuated Total Reflectance Fourier Transform-Infrared Spectroscopy (ATR FTIR) was performed using a Nicolet FTIR 6700 spectrophotometer equipped with a Smart Miracle single bounce diamond ATR accessory (Thermo Fisher Scientific, Waltham, MA). The data collection was completed using OMNIC 2.1 software. Before measurement, Ag−lyso preparations were centrifuged at 14000*g* for 20 min and supernatants were removed to concentrate the nanoparticles. For ATR FTIR of lysozyme, 10 μL of a lysozyme stock powder slurry in methanol was dried on the instrument crystal before measurement. Hydrolase activity of lysozyme in lyso−Ag preparations was determined colorimetrically by using the substrate (PNP-$(GlcNAc)_5$), as previously described.[48] For these activity assays, lysozyme−silver nanoparticles were made using 5 mg mL^{-1} lysozyme, and the synthesis reaction was completed in 50% methanol. Methanol interferes with the hydrolytic assay and the increased lysozyme concentration and lower methanol content allowed for measurable activity within the limits of the assay after a necessary 1000-fold dilution into the activity assay buffer.

Antimicrobial Activity Assays. The following strains used in the antimicrobial assays were obtained from American type Culture Collection (ATCC, Manassas, VA): *Escherichia coli* (ATCC 25922), *Staphylococcus aureus* (ATCC 25923) and *Candida albicans* (ATCC 10231). *Bacillus anthracis* Sterne strain 34F2 was isolated from a veterinary vaccine culture, supplied by Colorado Serum Company, Denver, CO.[49] *E. coli* strains J53 and J53(pMG101) and *P. mirabilis* strains LST149 and LST169A were gifts from Dr. Anne O. Summers at the Microbiology Department, University of Georgia, Athens, GA. Luria−Bertani and yeast mold media were used to grow silver-sensitive bacterial strains and *C. albicans*, respectively, in liquid and on solid media plates (plates contained 1% agarose) (Difco Laboratories, Sparks, MD). Luria−Bertani media was also used to grow silver-resistant bacteria strains, except NaCl was omitted and the media was supplemented with either 100 mg L^{-1} silver acetate for the LST strains or 100 mg L^{-1} ampicillin for J53(pMG101) to maintain silver resistance phenotypes. Antimicrobial assays to determine MIC values were completed according to the broth microdilution method.[50] Actively growing cultures (log phase growth) were diluted into fresh Mueller−Hinton media (Difco) to a concentration of 10^5 cells mL^{-1}. Initial viable cell counts were confirmed by growing serial dilutions of cultures on solid growth media. The cell suspensions were dispensed into a polypropylene 96-well microtiter plate (50 μL per well). Dilutions of the Ag−lyso preparations were then added to each well (50 μL) and incubated for 24 h at 37 °C. The microtiter plates were gently agitated during incubation using a rotary tabletop shaker (100 rpm). The MIC was recorded as the lowest concentration of silver in which no visible growth could be observed. Standard deviations in the results section represent at least three independent assays and each assay was completed in triplicate.

Atomic force microscopic (AFM) images of *B. anthracis* cultures incubated with and without Ag−$lyso_{25k}$ nanoparticles were obtained using a Nanoscope V, equipped with a Multimode V scanning probe microscope and a PicoForce stage (Veeco Instruments Inc., Woodbury, NY). Cells were grown as described above either containing a concentration of Ag−lyso nanoparticles at the MIC or with no nanoparticles. A few microliters of each cell culture were spread onto 5 mm square silicon wafers and dried at 37 °C for 5 min before imaging in tapping mode, using an etched phosphorus (*n*) doped silicon cantilever probe (type RTESP, Veeco). For pictures of whole cells, amplitude images showing topography and amplitude error images, which enhance cell surface edges, were overlaid to form a composite image using Photoshop CS2 by Adobe Systems Inc. (San Jose, CA). The enhanced images are subjective and show topography while able to outline fine detail simultaneously.

Cytotoxicity Assays. The cytotoxicity of silver nanoparticles was measured by monitoring the number of viable human keratinocyte cells after incubation in the presence of Ag−$lyso_{25k}$ preparations. The human epidermal keratinocyte cell line (HaCaT) was generously donated by the Army Research Laboratory.[51] Cells were cultured in a flask with RPMI-1640 media (ATCC) supplemented with 10% fetal bovine serum (ATCC) and 1% penicillin/streptomycin (Sigma) and incubated at 37 °C in a humidified incubator with 5% CO_2. For the cytotoxicity assays, cells were added to 96 well plates (5×10^3 cells per well) and incubated at 37 °C with 5% CO_2 for 48 h until approximately 80% confluent. The same media was used as described above except serum was not added to the cultures. After reaching confluency, cells were treated with various concentrations of Ag−$lyso_{25k}$ and allowed to incubate an additional 24 h. The addition of water to cells served as negative controls. After 24 h the Ag−lyso nanoparticles were removed from the wells and the cells were washed three times with phosphate-buffered saline (PBS) to remove residual nanoparticles. To determine the viability of cells in each well, metabolic activity was measured using the CellTiter 96 AQueous One Solution Assay (Promega, Madison, WI) according to the manufacturer's instructions. Culture media (100 μL) was added back to each well containing washed cells, followed by 20 μL of the AQueous One Solution reagent. After 3 h incubation, the absorbance was measured at 490 nm with a standard microplate reader (SpectraMAX GeminiXS, Molecular Devices, Sunnyvale, CA). Each experiment was done in triplicate. The relative cell viability (%) related to control wells containing cell culture medium without nanoparticles or PBS as a vehicle was calculated by $[A]_{test}/[A]_{control}$ multiplied by 100, where $[A]_{test}$ is the absorbance of the test sample and $[A]_{control}$ is the absorbance of control sample. All experiments were done in triplicate and the results from three different batches of Ag−$lyso_{25k}$ nanoparticles were averaged to give an overall assessment of toxicity. The experimental data were analyzed by Student's *t* test, and statistical significance was defined as $p < 0.05$.

Acknowledgment. We thank S. Sizemore for assistance in antimicrobial assays, H. Luckarift and L. Nadeau for useful discussions, and K. Kelly at University of Florida, Gainesville, FL, for TEM images. Research was supported by funding from Air Force Materials and Manufacturing Directorate (AFRL/RXQL; D.M.E., K.E.F., and G.R.J.), the Henry Jackson Foundation (N.M.S.), and the Joint Science and Technology Office, Defense Threat Reduction Agency, under Project Codes AA06CBT008 (D.M.E., K.E.F., and G.R.J.) and 4.1003607AHBB (N.M.S. and S.M.H.).

Supporting Information Available: TEM images and absorbance spectrum of the silver acetate and lysozyme reaction mixture in water; ATR FTIR spectra of Ag−lyso nanoparticle preparations; size distribution of Ag−$lyso_{25k}$ preparations calculated from TEM images; TEM images of aqueous Ag−lyso preparations. This material is available free of charge *via* the Internet at http://pubs.acs.org.

REFERENCES AND NOTES

1. Silver, S.; Phung, L. T.; Silver, G. Silver as Biocides in Burn and Wound Dressings and Bacterial Resistance to Silver Compounds. *J. Ind. Microbiol. Biotechnol.* **2006**, *33*, 627–634.
2. Chen, X.; Schluesener, H. J. Nanosilver: A Nanoproduct in Medical Application. *Toxicol. Lett.* **2008**, *176*, 1–12.
3. Dibrov, P.; Dzioba, J.; Gosink, K. K.; Hase, C. C. Chemiosmotic Mechanism of Antimicrobial Activity of Ag(+) in *Vibrio cholerae*. *Antimicrob. Agents Chemother.* **2002**, *46*, 2668–2670.
4. Feng, Q. L.; Wu, J.; Chen, G. Q.; Cui, F. Z.; Kim, T. N.; Kim, J. O. A Mechanistic Study of the Antibacterial Effect of Silver Ions on *Escherichia coli* and *Staphylococcus aureus*. *J. Biomed. Mater. Res.* **2000**, *52*, 662–668.
5. Lok, C. N.; Ho, C. M.; Chen, R.; He, Q. Y.; Yu, W. Y.; Sun, H.; Tam, P. K.; Chiu, J. F.; Che, C. M. Silver Nanoparticles: Partial Oxidation and Antibacterial Activities. *J. Biol. Inorg. Chem.* **2007**, *12*, 527–534.
6. Lansdown, A. B. G. Silver in Health Care: Antimicrobial Effects and Safety in Use. *Curr. Probl. Dermatol.* **2006**, *33*, 17–34.
7. Lok, C. N.; Ho, C. M.; Chen, R.; He, Q. Y.; Yu, W. Y.; Sun, H.; Tam, P. K.; Chiu, J. F.; Che, C. M. Proteomic Analysis of the Mode of Antibacterial Action of Silver Nanoparticles. *J. Proteome Res.* **2006**, *5*, 916–924.
8. Sondi, I.; Salopek-Sondi, B. Silver Nanoparticles as Antimicrobial Agent: A Case Study on *E. coli* as a Model for Gram-Negative Bacteria. *J. Colloid Interface Sci.* **2004**, *275*, 177–182.
9. Li, Y.; Leung, P.; Yao, L.; Song, Q. W.; Newton, E. Antimicrobial Effect of Surgical Masks Coated with Nanoparticles. *J. Hosp. Infect.* **2006**, *62*, 58–63.
10. Strohal, R.; Schelling, M.; Takacs, M.; Jurecka, W.; Gruber, U.; Offner, F. Nanocrystalline Silver Dressings as an Efficient Anti-MRSA Barrier: A New Solution to an Increasing Problem. *J. Hosp. Infect.* **2005**, *60*, 226–230.
11. Zhang, W.; Qiao, X.; Chen, J. Synthesis of Silver Nanoparticles--Effects of Concerned Parameters in Water/Oil Microemulsion. *Mater. Sci. Eng., B* **2007**, *142*, 1–15.
12. Mandal, D.; Bolander, M. E.; Mukhopadhyay, D.; Sarkar, G.; Mukherjee, P. The Use of Microorganisms for the Formation of Metal Nanoparticles and Their Application. *Appl. Microbiol. Biotechnol.* **2006**, *69*, 485–492.

13. Mohanpuria, P.; Rana, N.; Yadav, S. Biosynthesis of Nanoparticles: Technological Concepts and Future Applications. *J. Nanopart. Res.* **2008**, *10*, 507–517.
14. Klaus, T.; Joerger, R.; Olsson, E.; Granqvist, C. G. Silver-Based Crystalline Nanoparticles, Microbially Fabricated. *Proc. Natl. Acad. Sci. U.S.A.* **1999**, *96*, 13611–13614.
15. Naik, R. R.; Stringer, S. J.; Agarwal, G.; Jones, S. E.; Stone, M. O. Biomimetic Synthesis and Patterning of Silver Nanoparticles. *Nat. Mater.* **2002**, *1*, 169–172.
16. Xie, J.; Lee, J. Y.; Wang, D. I. C.; Ting, Y. P. Silver Nanoplates: From Biological to Biomimetic Synthesis. *ACS Nano* **2007**, *1*, 429–439.
17. Nam, K. T; Lee, Y. J.; Krauland, E. M.; Kottmann, S. T.; Belcher, A. M. Peptide-Mediated Reduction of Silver Ions on Engineered Biological Scaffolds. *ACS Nano* **2008**, *2*, 1480–1486.
18. Luckarift, H. R.; Dickerson, M. B.; Sandhage, K. H.; Spain, J. C. Rapid, Room-Temperature Synthesis of Antibacterial Bionanocomposites of Lysozyme with Amorphous Silica or Titania. *Small* **2006**, *2*, 640–643.
19. Mock, J. J.; Barbic, M.; Smith, D. R.; Schultz, D. A.; Schultz, S. Shape Effects in Plasmon Resonance of Individual Colloidal Silver Nanoparticles. *J. Chem. Phys.* **2002**, *116*, 6755–6759.
20. Chen, M.; Feng, Y. G.; Wang, X.; Li, T. C.; Zhang, J. Y.; Qian, D. J. Silver Nanoparticles Capped by Oleylamine: Formation, Growth, and Self-Organization. *Langmuir* **2007**, *23*, 5296–5304.
21. Haggerty, L.; Lenhoff, A. M. Analysis of Ordered Arrays of Adsorbed Lysozyme by Scanning Tunneling Microscopy. *Biophys. J.* **1993**, *64*, 886–895.
22. Schmidt, C. F.; Zimmermann, R. M.; Gaub, H. E. Multilayer Adsorption of Lysozyme on a Hydrophobic Substrate. *Biophys. J.* **1990**, *57*, 577–588.
23. Sethuraman, A.; Belfort, G. Protein Structural Perturbation and Aggregation on Homogeneous Surfaces. *Biophys. J.* **2005**, *88*, 1322–1333.
24. Luckarift, H. R.; Balasubramanian, S.; Paliwal, S.; Johnson, G. R.; Simonian, A. L. Enzyme-Encapsulated Silica Monolayers for Rapid Functionalization of a Gold Surface. *Colloids Surf. B* **2007**, *58*, 28–33.
25. Gittins, D. I.; Caruso, F. Biological and Physical Applications of Water-Based Metal Nanoparticles Synthesised in Organic Solution. *Chem. Phys. Chem.* **2002**, *3*, 110–113.
26. Wangoo, N.; Bhasin, K. K.; Boro, R.; Suri, C. R. Facile Synthesis and Functionalization of Water-Soluble Gold Nanoparticles for a Bioprobe. *Anal. Chim. Acta* **2008**, *610*, 142–148.
27. Yang, T.; Li, Z.; Wang, L.; Guo, C.; Sun, Y. Synthesis, Characterization, and Self-Assembly of Protein Lysozyme Monolayer-Stabilized Gold Nanoparticles. *Langmuir* **2007**, *23*, 10533–10538.
28. Vertelov, G. K.; Yu, A. K.; Efremenkova, O. V.; Olenin, A. Y.; Lisichkin, G. V. A Versatile Synthesis of Highly Bactericidal Myramistin® Stabilized Silver Nanoparticles. *Nanotechnology* **2008**, *19*, 355707.
29. Soukupová, J.; Kvítek, L.; Panáček, A.; Nevěčná, T.; Zbořil, R. Comprehensive Study on Surfactant Role on Silver Nanoparticles (NPs) Prepared *via* Modified Tollens Process. *Mater. Chem. Phys.* **2008**, *111*, 77–81.
30. Radmacher, M.; Fritz, M.; Hansma, H. G.; Hansma, P. K. Direct Observation of Enzyme Activity with the Atomic Force Microscope. *Science* **1994**, *265*, 1577–1579.
31. Kamatari, Y. O.; Konno, T.; Kataoka, M.; Akasaka, K. The Methanol-Induced Transition and the Expanded Helical Conformation in Hen Lysozyme. *Protein Sci.* **1998**, *7*, 681–688.
32. Schierholz, J. M.; Lucas, L. J.; Rump, A.; Pulverer, G. Efficacy of Silver-Coated Medical Devices. *J. Hosp. Infect.* **1998**, *40*, 257–262.
33. Pal, S.; Tak, Y. K.; Song, J. M. Does Antibacterial Activity of Silver Nanoparticle Depend on Shape of Nanoparticle? A Study on Gram-Negative *E. coli*. *Appl. Environ. Microbiol.* **2007**, *73*, 1712–1720.
34. Panáček, A.; Kvítek, L.; Prucek, R.; Kolář, M.; Večeřová, R.; Pizúrová, N.; Sharma, V. K.; Nevěčna, T.; Zbořil, R. Silver Colloid Nanoparticles: Synthesis, Characterization, and Their Antibacterial Activity. *J. Phys. Chem. B* **2006**, *110*, 16248–16253.
35. Arora, S.; Jain, J.; Rajwade, J. M.; Paknikar, K. M. Cellular Responses Induced by Silver Nanoparticles: *In Vitro* Studies. *Toxicol. Lett.* **2008**, *179*, 93–100.
36. Braydich-Stolle, L.; Hussain, S.; Schlager, J. J.; Hofmann, M. C. *In Vitro* Cytotoxicity of Nanoparticles in Mammalian Germline Stem Cells. *Toxicol. Sci.* **2005**, *88*, 412–419.
37. Schrand, A. M.; Braydich-Stolle, L. K.; Schlager, J. J.; Dai, L.; Hussain, S. M. Can Silver Nanoparticles Be Useful as Biological Labels. *Nanotechnology* **2008**, *19*, 235104.
38. Asharani, P. V.; Mun, G. L. K.; Hande, M. P. Valiyaveettil. Cytotoxicity and Genotoxicity of Silver Nanoparticles in Human Cells. *ACS Nano* **2009**, *3*, 279–290.
39. Nepal, D.; Geckeler, K. E. pH-Sensitive Dispersion and Debundling of Single-Walled Carbon Nanotubes: Lysozyme as a Tool. *Small* **2006**, *2*, 406–412.
40. Knubovets, T.; Osterhout, J. J.; Klibanov, A. M. Structure of Lysozyme Dissolved in Neat Organic Solvents as Assessed by NMR and CD Spectroscopies. *Biotechnol. Bioeng.* **1999**, *63*, 242–248.
41. Kato, S.; Okamura, M.; Shimamoto, N.; Utiyama, H. Spectral Evidence for a Rapidly Formed Structural Intermediate in the Refolding Kinetics of Hen Egg-White Lysozyme. *Biochemistry* **1981**, *20*, 1080–1085.
42. Jacoben, S. M.; Stickler, D. J.; Mobley, H. L. T.; Shirtliff, M. E. Complicated Catheter-Associated Urinary Tract Infections Due to *Escherichia coli* and *Proteus mirabilis*. *Clin. Microbiol. Rev.* **2008**, *21*, 26–59.
43. Wireman, J.; Liebert, C. A.; Smith, T.; Summers, A. O. Association of Mercury Resistance with Antibiotic Resistance in the Gram-Negative Fecal Bacteria of Primates. *Appl. Environ. Microbiol.* **1997**, *63*, 4494–4503.
44. Summers, A. O.; Wireman, J.; Vimy, M. J.; Lorscheider, F. L.; Marshall, B.; Levy, S. B.; Bennett, S.; Billard, L. Mercury Released From Dental "Silver" Fillings Provokes an Increase in Mercury- and Antibiotic-Resistant Bacteria in Oral and Intestinal Floras of Primates. *Antimicrob. Agents Chemother.* **1993**, *37*, 825–834.
45. Gupta, A.; Phung, L. T.; Taylor, D. E.; Silver, S. Diversity of Silver Resistance Genes in IncH Incompatibility Group Plasmids. *Microbiology* **2001**, *147*, 3393–3402.
46. Summers, A. O. Genetic Linkage and Horizontal Gene Transfer, the Roots of the Antibiotic Multi-Resistance Problem. *Anim. Biotechnol.* **2006**, *17*, 125–135.
47. Silver, S. Bacterial Silver Resistance: Molecular Biology and Uses and Misuses of Silver Compounds. *FEMS Microbiol. Rev.* **2003**, *27*, 341–353.
48. Nanjo, F.; Sakai, K.; Usui, T. *p*-Nitrophenyl Penta-*N*-acetyl-beta-chitopentaoside as a Novel Synthetic Substrate for the Colorimetric Assay of Lysozyme. *J. Biochem.* **1988**, *104*, 255–258.
49. Ireland, J. A.; Hanna, P. C. Macrophage-Enhanced Germination of *Bacillus anthracis* Endospores Requires GerS. *Infect. Immun.* **2002**, *70*, 5870–5872.
50. Wiegand, I.; Hilpert, K.; Hancock, R. E. Agar and Broth Dilution Methods to Determine the Minimal Inhibitory Concentration (MIC) of Antimicrobial Substances. *Nat. Protoc.* **2008**, *3*, 163–175.
51. Boukamp, P.; Petrussevska, R. T.; Breitkreutz, D.; Hornung, J.; Markham, A.; Fusenig, N. E. Normal Keratinization in a Spontaneously Immortalized Aneuploid Human Keratinocyte Cell Line. *J. Cell Biol.* **1988**, *106*, 761–771.